PACS: 66.20.Fe

S.A.A. Akbari Mousavi[1], A.R. Shahab[2], M. Mastoori[3]

THREE-DIMENSIONAL NUMERICAL ANALYSIS OF TWIST EXTRUSION PROCESS FOR ANNEALED COPPER

[1]School of Metallurgy and Materials Engineering of Teheran

[2]School College of Engineering of Teheran

[3]University of Teheran
Teheran, Iran, P.O. Box: 11365-4563
E-mail: mousavi@engmail.ut.ac.ir, amshahab@ut.ac.ir, m_mastoori@yahoo.com

Nowadays in order to achieve the materials with superior strength and appropriate formability, severe plastic deformation (SPD) methods are used in which the available coarse-grained materials are processed to produce substantial grain refinement and a nanostructure. A new SPD method based on direct extrusion process, proposed recently, is the «Twist Extrusion process». The process is capable of industrial usage and has the advantage of producing a finer structure as compared with other SPD methods. In this investigation, in order to help in determining the effective process variables and in understanding the die manufacturing process, the simulation of the twist extrusion process is presented by using explicit analysis procedure, and the von-Misses and equivalent plastic, strain distributions are considered. The effects of friction coefficient and speed of deformation on the maximum values of von-Misses stress and equivalent plastic strain for the annealed copper material are investigated, they are validated and compared with the corresponding theoretical and experimental values obtained from researchers. The simulation results show that the maximum and minimum equivalent plastic strains are produced at the corner and at the center of the billet, respectively. The maximum and minimum equivalent plastic strains predicted by the simulations are found to be 1.3 and 0.3, respectively. Serrated diagrams of instantaneous stress versus strain and applicable flow stress were observed and recalculated. Simulation results placed next to experimental results are indicative of an acceptable level of compatibility.

1. Introduction

The severe plastic deformation process is the most effective method to obtain ultrafine grained materials. The known SPD processes are: equal channel angular extrusion (ECAE), accumulative roll bonding (ARB), high-pressure torsion (HPT) and multiple forging [1–3].

A new SPD method proposed recently is the twist extrusion process [4]. In this method, a square section billet is pressed into a 90-deg twisted channel of

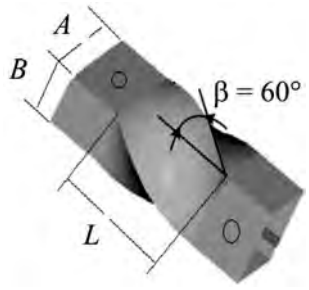

Fig. 1. Schematic of the twist extrusion process [10]

Fig. 2. Photo of mechanical twist extrusion process in the cold state condition [9]

extrusion die. Twist extrusion product during the process is schematically shown in Fig. 1. Moreover, the cross-section of the billet during the 90-deg rotation is constant. The geometry of the cross-section of billet is chosen arbitrarily but not circular. A very high magnitude of strain is produced during deformation. Since in this process the cross-section is constant, it is possible to perform this process in more than one pass and accumulate strains in order to produce the finer grains in the bulk structure [4–7]. For instance, three passes of twist extrusion on pure titanium, achieving less than 1 μm grain [7]; it is also possible to produce pure copper with 100 nm grain size [8]. Different technological schemes can be used to exert high pressure on the specimen. The mechanical cold type scheme modeled in this study is shown in Fig. 2.

A detailed analysis and understanding of the mechanism of the process are not possible on the basis of conventional observations because the twist extrusion process is very complicated. Hence, for the mechanism of twist extrusion to be more perceptive, the finite element analysis was performed by using the explicit analysis procedure. Till now, the efficiency of FEM analyses in prediction and optimization of this process has not been approved [4].

In this investigation, simulations of twist extrusion process in cold state condition for annealed copper (T = 500°C, 4 h) is presented. The effective strain and von-Misses stress distribution are considered by using ABAQUS 6.4-PR11 software. In addition, the maximum values of effective strain obtained during deformation are compared and validated with the corresponding experimental values of Refs. [8,10]. In addition, the effective strain distribution along 4 different paths of the sample is considered.

2. Simulation of the twist extrusion process

In this study, two types of the annealed copper samples with the cross-section of 18 × 28 mm and lengths of 30 and 55 mm are used. For the 55 mm sample, a guide is required to avoid bulging during the process. Ram speed used is 5 mm/s and friction coefficient between the die and sample surfaces is chosen to be 0.1. The maximum applied pressure is 400 MPa. The die and ram are modeled as rigid solid type. The die, punch and data specifications are chosen as in Refs. [8–10].

The Hollowman elastic-plastic equation is used to describe the behavior of billet (i.e. $\sigma = c\varepsilon^n$, where σ is stress, ε is strain and n is the strain-hardening constant, c and n are material constants). The material constants used are c = 525 MPa,

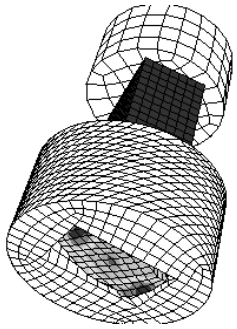

Fig. 3. Schematic of the twist extrusion process during deformation (simulation results)

n = 0.38 [3]. All the simulations are carried out with annealed copper (ρ = 8900 kg/m^3, E = 124 GPa, ν = 0.34, σ_y = 50 MPa, k = 160 MPa)**.** Frictional shear stress τ for all of the contact surfaces is defined as: $\tau = mk$, where m is a friction factor and k is a shear flow of material. A friction factor of m = 0.1 is considered for all contact surfaces. Mechanical properties of annealed copper are the same as those reported in Refs. [8–10].

Explicit method is selected to solve equations in order to consider large deformations. The billet and die contact is modeled with friction surface to surface finite sliding contact pair algorithm. The frictional form of this algorithm was also used to model the ram contact with billet. Die and billet contact surface is chosen to be separable and ram and billet contact is chosen to be not separable.

Boundary conditions were chosen to be like experimental ones; therefore the six degree of freedom of die is foreclosed and ram could move only in direction normal to billet during the deformation. The billet mesh size is chosen to be 1 mm.

3. Simulation results and discussion

Fig. 3 shows schematic of the setup used for simulation. Figs. 4,*a* and 5,*a* show the longitudinal and end view cross-section of simulated sample after deformation, respectively. Figs. 4,*b* and 5,*b* show the longitudinal and end view cross-section of experimental sample after deformation from Ref. [9]. Comparing these figures shows a close conformity between simulation results and experimental observations. The simulation results are capable of predicting the defects in the longitudinal direction and corners of the twist end cross-section.

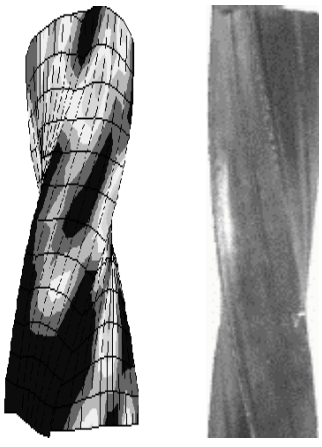

a *b*

Fig. 4. Schematic (simulation results) (*a*) and photo (experimental results [9]) (*b*) of twist sample after one-pass deformation

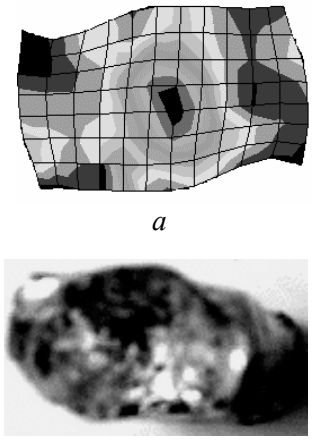

a

b

Fig. 5. Schematic (simulation results) (*a*) and photo (experimental results [9]) (*b*) of end view cross-section of sample after deformation

3.1. The von-Misses stress profiles

Figs. 6,*a–d* show the von-Misses stress profiles along the central line axis of the sample at the end of 1/4, 1/2, 3/4 and 1 total deformation time, respectively. The figures show that only one maximum stress occurred at a particular position along the central line of the specimen. The maximum stress achieved is found to be 400 MPa. In addition, the position of the maximum stress along the 55 mm billet is changing towards the end of the billet. It should be noted that in these figures, the die entrance is at the right-hand side of the diagram.

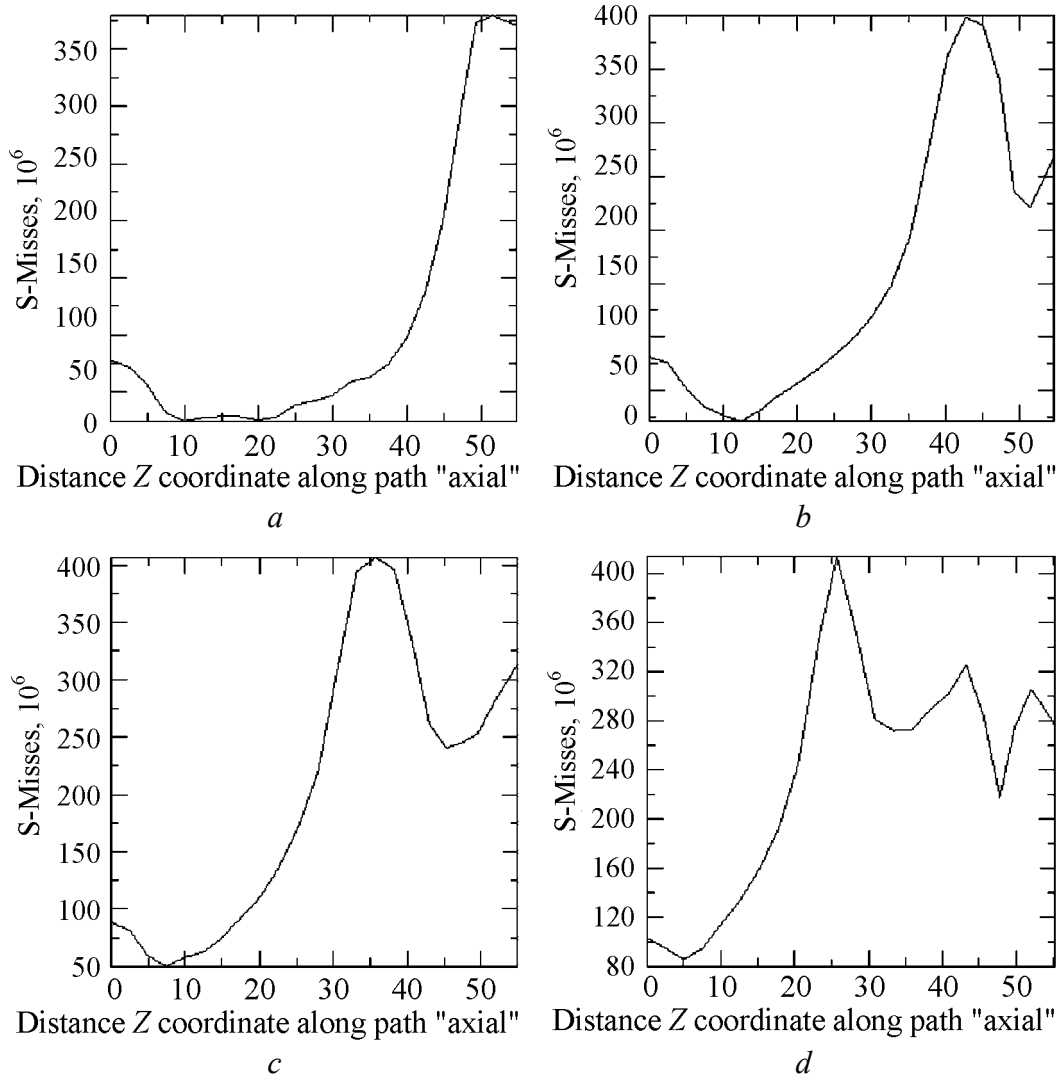

Fig. 6. The von-Misses stress profiles along the central line axis of the sample at the end of 1/4 (*a*), 1/2 (*b*), 3/4 (*c*) and 1 total (*d*) deformation time

Fig. 7 illustrates variation of von-Misses stress versus time for the middle point of axial path in one-pass deformation. The figure shows that during the process, stress increases to a maximum value and then decreases. The maximum value of the von-Misses stress is found to be about 400 MPa. The trend of diagram and the

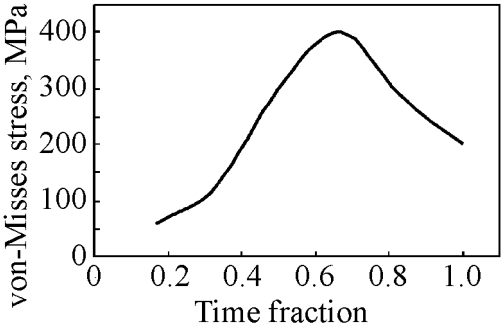

Fig. 7. Variation of von-Misses stress against time for the middle point of axial path during one-pass deformation

maximum magnitude are in a close compatibility with the corresponding experimental value reported in Ref. [9] when the back pressure is not applied.

The maximum stress profiles required for deformation of two simultaneous passes are shown in Fig. 8. The simulated product after two consecutive passes is depicted in Fig. 9. The simulation results predicted a maximum stress of 500 MPa required for deformation. This maximum value is greater than that needed for one-pass deformation (400 MPa). The maximum stress value is comparable to experimental stress reported in Ref. [8]. The figure also shows a periodicity of the stress due to strain accumulation and grain refinement and relaxation of internal stress.

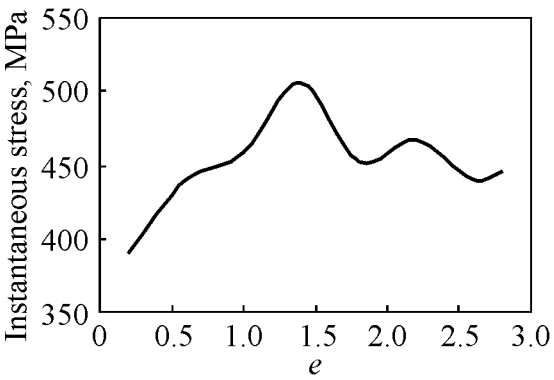

Fig. 8. Instantaneous maximum stress in whole body of the sample in two passes of deformation vs strain

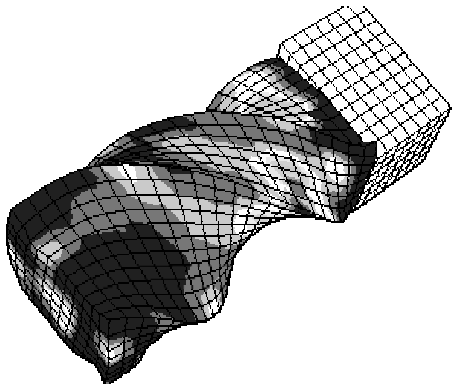

Fig. 9. Schematic of product after two simultaneous passes

As noted in previous diagrams of the article, the maximum resistant stress against deformation in one pass is estimated to be about 400 MPa. This value can be substituted as σ_s in the equation derived from kinematically admissible velocity fields from Ref. [9]:

$$P = \frac{4\sigma_s}{3\sqrt{3}} \mathrm{tg}\beta_{\max} + \frac{2\sigma_s fh}{\sqrt{3}\cos\beta_{\max} R}, \qquad (1)$$

where P – flow stress (press applicable power), σ_s – resistant stress of material against deformation, $\beta_{\max}$ – maximum magnitude of inclination of twisted line against axes of extrusion, f – friction coefficient, h/R – specific ratio dependent on die geometry.

By substituting σ_s = 400 MPa in this formula, the applicable working pressure is found to be equal to 1200 MPa. By inclusion of back pressure, the maximum working pressure obtained is 1800 MPa, in close agreement with that reported in Ref. [8] e.g. 2000 MPa.

3.2. The equivalent strain distributions

The equivalent strain contours at the end of 1/4, 1/2, 3/4 and 1 total deformation time are shown in Figs. 10,*a–d*, respectively. The maximum effective strain obtained from the simulation at the end of the one pass is 1.5 which is compatible with experimental results of Ref. [8]. This validates the simulations.

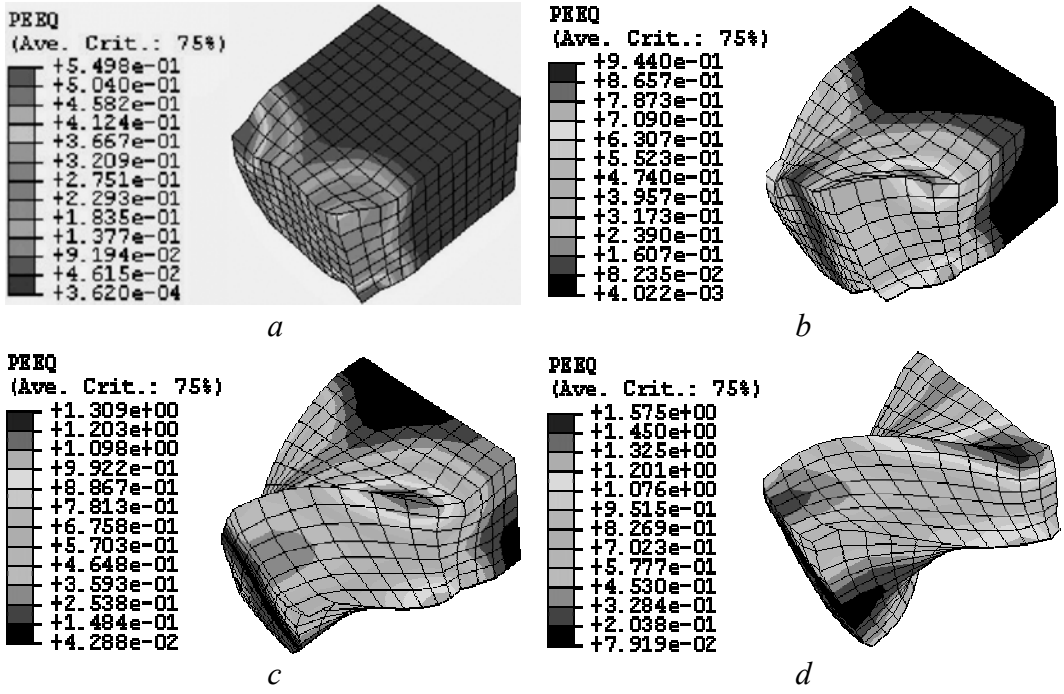

Fig. 10. The equivalent strain contours at the end of 1/4 (*a*), 1/2 (*b*), 3/4 (*c*) and 1 total (*d*) deformation time

It was noted in the literature that the grain size is dependent upon the magnitude of effective strain imposed on the sample. Therefore, further study is conducted to consider the variation of strains in the sample during the deformation. The change of induced strain during deformation results in mechanical anisotropy and grain size differences in experimental data.

Figs. 11,*a–d* show the effective strain profiles along the corner axis of the sample at the end of 1/4, 1/2, 3/4 and 1 total deformation time, respectively. The figures show that only one maximum strain occurred at a particular position along the central line of the specimen. The maximum strain achieved is found to be 0.3 in the center line, 0.45 in the mid-length (28 mm), 1 in the mid-width (18 mm) and 1.3 at the corners. In addition, the position of the maximum strain along the 55 mm billet is changing towards the end of the billet. It should be noted that the die entrance is at the right-hand side of the figures.

3.3. Effects of ram speed on the effective strain profiles

Further study is conducted to consider the effect of ram speed on the magnitude of maximum plastic strain induced during the process. The simulation results show that increasing the punch speed from 5 mm/s to 10 mm/s results in increasing the magnitudes of the effective strain from 1.3 to 1.5 (see Fig. 12).

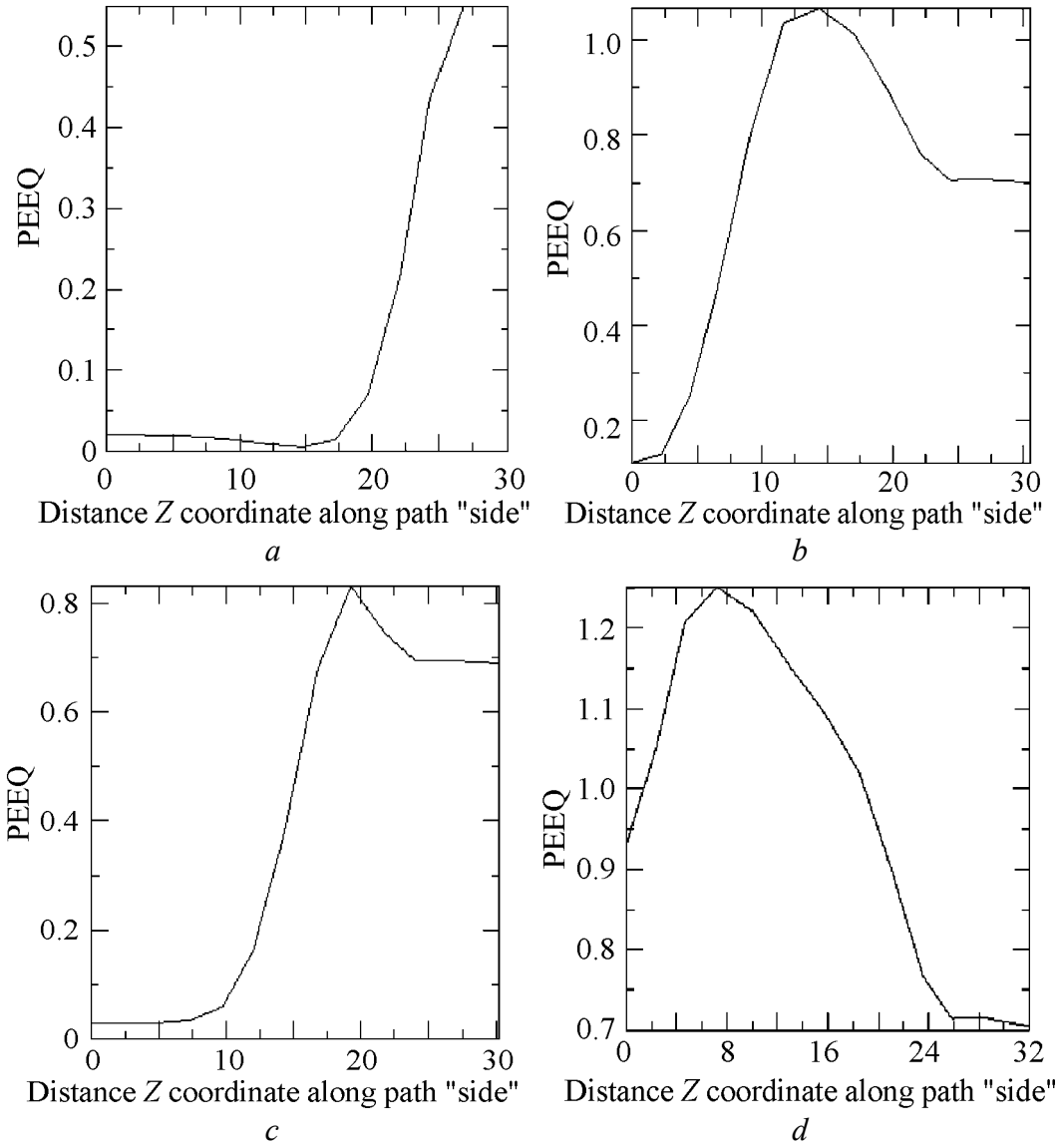

Fig. 11. The effective strain profiles along the corner axis of the sample at the end of 1/4 (*a*), 1/2 (*b*), 3/4 (*c*) and 1 total (*d*) deformation time

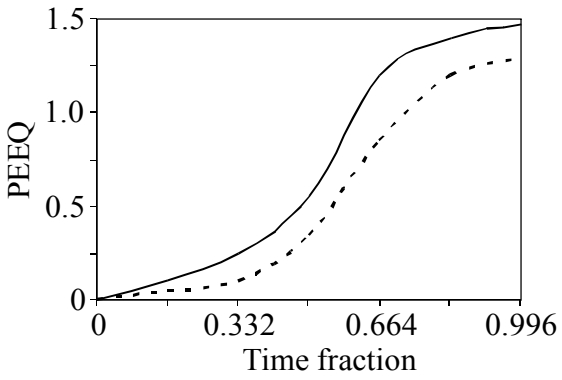

Fig. 12. Effective strain profile for the ram speeds of 5 mm/s (dashed line) and 10 mm/s (solid line) vs. time fraction of 1/6

3.4. Effect of friction coefficient on the effective strain profiles

Simulation results show that the von-Misses stress distributions change by increasing the friction coefficient (see Figs. 13 and 14). In addition, the simulation results show that the positions of maximum and minimum stresses move further along the sample toward the exit. Moreover, the minimum stress obtained for the friction coefficient of 0.2 is less than that of 0.1 (see Figs. 14 and 6,*d*).

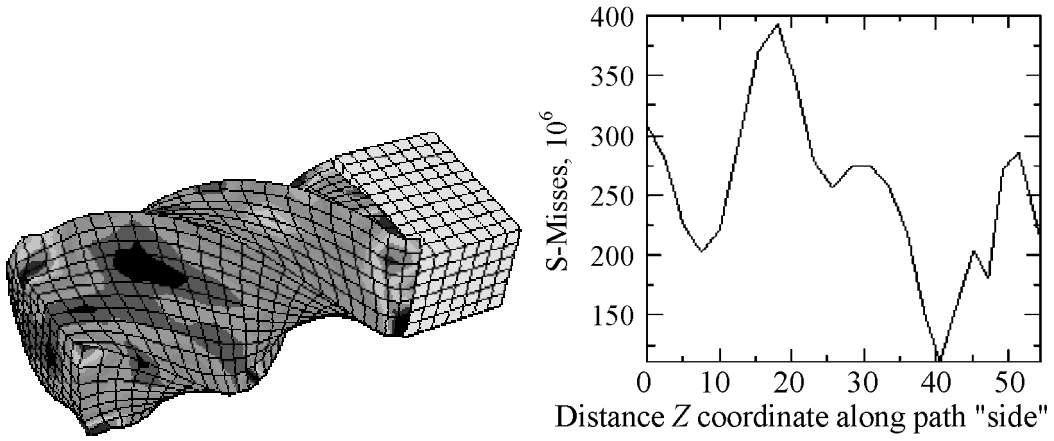

Fig. 13. Schematic of von-Misses stress contour type of sample (friction coefficient of 0.2) (*a*) and the von-Misses stress profiles along the corner axis of the sample at the end of total deformation time (friction coefficient of 0.2) (*b*) (compared with Fig. 6,*d*)

4. Conclusion

The deformed shape and the end view cross-section of sample achieved from the simulation are in complete agreement with those of experiments.

The simulations results predicted that the maximum values of plastic strain reach 1.3. The data is compatible with values of 1.2–1.5 obtained from the experimental data of Refs. [8–10]. This matter validates the simulation results.

The results show that the maximum and minimum effective strains are achieved at the corner and at the center of the specimen, respectively.

The results show that the effective strain increases with the ram speed.

The maximum working pressure obtained from the numerical analyses is in reasonable agreement with that obtained from the upper band analyses of reference [8,9].

The position of maximum and minimum flow stress moves toward the exit by increasing the friction coefficient.

1. *R.Z. Valiev, R.K. Islamgaliev, I.V. Alexandrov*, Prog. Mat. Sci. **45**, 102 (2000).
2. *Y. Saito, H. Utsunomiya, N. Tsuji, T. Sakai*, Acta mater **47**, 579 (1999).
3. *Y. Iwahashi, Z. Horita, M. Nemoto, T.G. Langdon*, Acta mater **45**, 4733 (1997).

4. *Y. Beygelzimer, D. Orlov, V. Varyukhin*, Ultrafine grained materials II, Y.T. Zhu, T.G. Langdon, R.S. Mishra, S.L. Semiatin, M.J. Saran, T.C. Lowe (eds.), TMS (2002), p. 297–304.
5. *Y. Beygelzimer, D. Orlov, V. Varyukhin, B. Efros,V. Stolyarov, H. Salimgareev*, Ultrafine grained materials II, Y.T. Zhu, T.G. Langdon, R.S. Mishra, S.L. Semiatin, M.J. Saran, T.C. Lowe (eds.), TMS (2002), p. 43–46.
6. *D. Orlov,V. Stolyarov, H. Salimgareyev, E. Soshnikova*, Ultrafine grained materials III, Y.T. Zhu, T.G. Langdon, R.Z. Valiev, S.L. Semiatin, D.H. Shin, T.C. Lowe (eds.), TMS (2004), p. 457–462.
7. *V.V. Stolyarov, Ya.E. Beigel'zimer, D.V. Orlov, R.Z. Valiev*, The Physics of Metals and Metallography **99**, 92 (2005).
8. *Y. Beygelzimer, D. Orlov, V. Varyukhin, S. Synkov, A. Spuskanyuk, Y. Pashinska*, Nanomaterials by severe plastic deformation, M.J. Zehetbauer, R.Z. Valiev (eds.), Wiley-VCH, Weinheim, Germany (2004), p. 511–516.
9. *Y. Beygelzimer, V. Varyukhin, D. Orlov, S. Synkov*, Twist extrusion – process for deformation accumulation, TEAN, Donetsk (Ukraine), 2003 [in Russian].
10. *Y. Beygelzimer, D. Orlov, V. Varyukhin, S. Synkov*, Application of Twist Extrusion, NANOSPD3 Conf., Japan (2005).
11. ABAQUS 6.4 Pro11 software, Help (2005).